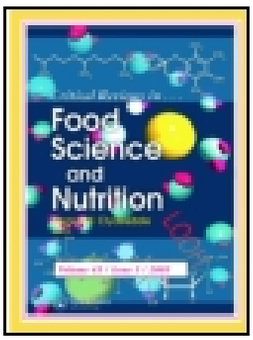

Taylor & Francis
Taylor & Francis Group

Critical Reviews in Food Science and Nutrition

ISSN: 1040-8398 (Print) 1549-7852 (Online) Journal homepage: http://www.tandfonline.com/loi/bfsn20

Atomic Force Microscopy of Starch Systems

Fan Zhu

To cite this article: Fan Zhu (2015): Atomic Force Microscopy of Starch Systems, Critical Reviews in Food Science and Nutrition, DOI: 10.1080/10408398.2015.1094650

To link to this article: http://dx.doi.org/10.1080/10408398.2015.1094650

Atomic force microscopy of starch systems

Fan Zhu

School of Chemical Sciences, University of Auckland, Private Bag 92019, Auckland 1142, New Zealand. Correspondence, e-mail: fzhu5@yahoo.com

Abstract

Atomic force microscopy (AFM) generates information on topography, adhesion, and elasticity of sample surface by touching with a tip. Under suitable experimental settings, AFM can image biopolymers of a few nanometres. Starch is a major food and industrial component. AFM has been used to probe the morphology, properties, modifications, and interactions of starches from diverse botanical origins at both micro- and nano-structural levels. The structural information obtained by AFM supports the blocklet structure of the granules, and provides qualitative and quantitative basis for some physicochemical properties of diverse starch systems. It becomes evident that AFM can complement other microscopic techniques to provide novel structural insights for starch systems.

Keywords: atomic force microscopy; starch, structure, surface, processing, structure-property relationship

Introduction

The atomic force microscopy (AFM) is a type of scanning probe microscopy. Instead of "looking" at the samples, AFM generates high resolution images by 'feeling' the sample surface with a sharp tip (Morris et al., 2010; 2011). The interactions between the tip and sample can be recorded to generate various images of the surface structure. At a specific image point, a force–distance curve at the single-molecule level (force spectroscopy) can be generated from the variations in the sample-tip interaction (Morris et al., 2011). The advantages of AFM over the most other microscopic techniques include high resolution capacity, minimal sample preparation (samples in near-native state), suitability for non-conductive samples, flexible imaging environment (in liquid or gas), and quantification of ultra-small structure (Morris et al., 2010; Liu et al., 2008). Since the invention in 1986, AFM has been a useful tool to probe surface properties of diverse biological materials such as cells and biomacromolecules (Binnig et al., 1986; Morris et al., 2010). During the last two decades, AFM has been extended to include the food systems (Morris et al., 2011).

Starch is a major component of various crops with an un-limited supply. In nature, starch exists as semi-crystalline granules (Pérez & Bertoft, 2010). It is widely used in diverse food and non-food industry in native and modified forms (BeMiller & Whistler, 2010). Understanding the structural basis for starch properties and the changes during starch processing and interactions allows us to better control the product quality, and to design starch systems in a rational manner (Morris et al., 2011; BeMiller & Whistler, 2010). AFM, complementing other microscopies, aids

to achieve these missions in starch applications. At a fundamental level, AFM also has revealed novel features of starch that previously have not been noted by other techniques.

The molecular and granular structures, physicochemical properties, and applications of starch have been reviewed in detail previously (Pérez & Bertoft, 2010; BeMiller & Whistler, 2010). The basics of AFM have also been covered in detail previously (Morris et al., 2010). This review starts with brief overviews on the basics of starch structure and properties as well as the principles of AFM imaging. AFM applications in starch structure, properties, modifications, and interactions are summarised. Examples using AFM-based force spectroscopy for starch systems are also provided. AFM images are selectively provided for better illustration.

Overview of starch structure

Starch is among the mostly-occurred natural carbohydrate polymers. On the molecular level, amylose and amylopectin are the two major chemical components. Amylose is mostly linear and smaller than the branched amylopectin. On the granular level, Starch granules are semi-crystalline with a size ranging from ~1–100 μm, depending on the source. The granules are composed of semi-crystalline spherical blocklets with a size of 10–500 nm in diameter, depending on their location in the granules and more on the starch source. On a more subtle level, the granules are built up of alternating amorphous and semi-crystalline growth rings (shells) with a thickness of 100–400 nm (Figure 1). The semi-crystalline shells have a periodicity of ~ 9–10 nm with the alternating amorphous and crystalline lamellae. The branching regions of amylopectin are arranged in a clustered fashion, and most contribute to the formation of the amorphous lamellar. The side chains of amylopectin clusters in the form of double helices form

the crystalline lamellae. These double helices are arranged in two specific manners in the granules which are A-type and B-type polymorph. C-type is a blend of A- and B-type polymorph. The amylose component is believed to be distributed in the amorphous regions of the granules (Gallant et al., 1997; Pérez & Bertoft, 2010).

In the presence of heat and water, the granules start to hydrate and swell with some components (mostly amylose) leaching and solubilizing. Further water up-taking and heating facilitate the disruption of crystallites and granules. The dis-ordering process of granular organization is termed gelatinization. When the gelatinized starch is cooled, the dis-ordered starch chains re-associate and re-crystallize. This re-ordering process is termed retrogradation. The gelatinization and retrogradation of starch are crucial for diverse applications, and are sometimes diversified by starch modification (BeMiller & Whistler, 2009). These properties are also determined by the interactions of starch with other components present. Understanding the structural changes during starch processing contributes to a better definition of the structure-functionality relationships, and AFM provides additional structural perspectives.

Overview of AFM principles

AFM images are obtained by measurement of the force on a sharp tip created by the proximity to the sample surface (Binnig et al., 1986) (Figure 2). Starch samples are fixed on freshly-cut surface of mica. During scanning, the movement/deflection of the tip which is fixed on a cantilever spring can be captured by a laser-based device. Recording the change of the deflection by a photon-detector in the course of scanning, a topographic image of sample is plotted. Based on the nature of the interactive force between the tip and sample, major scanning modes of AFM

include contact dc mode, deflection mode, and non-contact ac mode and tapping ac mode (Morris et al., 2010; Liu et al., 2008). For the contact dc mode, there is direct contact between AFM tip and sample surface, and the interactive force is repulsive in nature. For the ac modes including tapping and non-contact modes, the interactive force between the tip and sample is attractive in nature which is weaker than the repulsive force in the contact mode. Non-contact mode is also referred to as the true non-contact mode where the tip never comes into contact with the sample. In the deflection mode, the gain of the system control loop is set to a lower value to make the response sluggish. Therefore, the image is not noted under a constant force, and a force map of sample is recorded. A variation of this mode is the error-signal mode. For the type of images obtained by AFM, there are three major ones including topography, frictional force (lateral force), and phase imaging. Topography imaging is most used for starch analysis to obtain the height information. The frictional force imaging is about the lateral deflections of the cantilever due to the forces on the cantilever parallel to the plane of the sample surface, and it records the variations in surface friction. Phase imaging records the phase lag between the cantilever oscillation output signal and signal driving the cantilever to oscillate. It can be used to detect the variations in properties such as adhesion and elasticity (Morris et al., 2010). These image types and the above-mentioned modes have both advantages and disadvantages for better image contrast, which depends on specific applications. They can be complementary to each other to obtain additional information. However, because of the high resolution capacity within a rather tiny scanning area and extreme sensitivity to changing conditions (e.g., thermal drift), artefacts of sample preparation and instrumental background noise may arise, demanding critical treatment of the data (Liu et al., 2008). Application of AFM in starch systems, not only have

confirmed previous results obtained by other microscopies, but also have revealed new features which have not been observed.

Structure of native starch granules

Surface structure

The size of native starch granules ranged from ~1–100 μm. It was suggested that starch granules are made up of blocklets with a size of 20 to 500nm which depends on their location in the granule and starch type (Gallant et al., 1997). Recent data of AFM continues to support the existence and structure of these blocklets of starch from diverse botanical sources such as Norway spruce needles (Cabálková et al., 2008), wheat (Waduge et al., 2013), potato (Baldwin et al., 1998), and mango (Simão et al., 2008) (Table 1). Difference in blocklet structure among diverse starches has been observed. For example, potato starch had more protrusions as blocklets on surface than wheat starch (Baldwin et al., 1998). Cassava starch had smoother surface than potato starch (Juszczak et al., 2003a). Apart from the blocklet structure, some other features of granule surface have been observed (Table 1). For example, starch granules of Norway spruce needles had both protrusions and furrows with pores (Cabálková et al., 2008). AFM has been used to probe the surface morphology of developing wheat starch granules (Waduge et al., 2010 and 2013). Surface roughness of starch granules decreased towards maturity. At early stages after anthesis, larger fuzzy blocklets were seen. These blocklets became smaller and less fuzzy towards maturity. At all stages, blocklets of small granules are larger and fuzzier with rougher surface than in large granules (Waduge et al., 2013).

Certain processing can reveal some structural features of granule surface by AFM. For example, rice starch was subjected to water plasticizing and lyophilisation. This cycle was repeated to destroy the hydrogen bonding in the granules. As a result, nano-particles of ~30 nm in diameter, which was resistant to further plasticizing/lyophilisation, were seen (Ayoub et al., 2006). They were suggested to be individual single cluster in the crystalline region of starch granules. It is rather tempting to imagine the possibility to isolate a single blocklet and analyse the structure, which seems a rather difficult task.

Internal structure

The internal part of starch granules can be exposed for AFM analysis. This has been achieved by sectioning of starch embedded in resin using an ultramicrotome (Ridout et al., 2004), glucoamylase hydrolysis (Ohtani et al., 2000), and physical destruction (milling) (Ohtani et al., 2000). Suitable sample preparation methods can increase the image resolution (Neethirajan et al., 2008; Ridout et al., 2004; Parker et al., 2008). Compared with sectioning using a microtome or enzymatic hydrolysis, physical destruction using a glass homogenizer appeared to be a better way to expose the inner part of granules for AFM imaging (Ohtani et al., 2000). UV/ozone treatment for 30s enhanced the resolution of AFM on starch granules from durum wheat to clearly show the growth ring structure, while plasma etching destroys all the areas of starch granules at a similar rate, thus helping little in AFM imaging (Neethirajan et al., 2008). It was apparent that crystalline and amorphous parts of starch granules had different susceptibility to UV/ozone oxidization and degradation. The sectioned samples were hydrated before AFM analysis for better image (Ridout et al., 2004; Parker et al., 2008; Tsukamoto et al., 2012). The

origin of the contrast in AFM images has been attributed to the differential absorption of water within localised and exposed fragments of the starch granules. The water absorption led to the swelling of the region which becomes higher than surrounding regions (Ridout et al., 2004). To avoid any artificial manipulation of the starch granules during isolation from the plant, internal granule structure was also examined *in situ* in dried pea seeds by using a standard ultramicrotome, and showed similar structure as the isolated starch (Parker et al., 2008).

AFM imaging of internal granule confirmed the hilum structure which tends to be much more amorphous than the outer layers (Baker et al., 2001; Ohtani et al., 2000; Ridout et al., 2006) (Figure 3). Blocklets exist continuously through starch granule (Parker et al., 2008). Fine particles of approximately 30 nm in diameter existed inside granules from diverse sources (Tsukamoto et al., 2012) (Figure 3). Growth ring structure under AFM may be visible or not, depending on the amount and presence of amylose in starches from specific pea mutants (Ridout et al., 2003; 2004; 2006). By analysing starches from pea mutants differing in amylose contents, it was suggested that amylose may form crystals that contribute to a fine, hard structure in the matrix where the blocklets sit (Ridout et al., 2003 and 2006). The presence of these amylose crystals may greatly decrease the water absorption and swelling of the regions, creating little image contrast for AFM. Polymorphism of starch could not be resolved by AFM as exemplified in starches from pea mutants (Ridout et al., 2006). Therefore, AFM is complementary to other techniques to gain a whole picture of starch structure.

Structure of starch biopolymer chains

AFM has been explored to image the starch polymer chains (Gunning et al., 2003; Maley et al., 2010). The sample preparation method appeared rather critical for gaining reasonable images of amylose and amylopectin chains (Maley et al., 2010; Li et al., 2009). The starch chains from gelatinized starch should be dispersed well to prevent any aggregation. By simply dropping gelatinized and diluted barley starch solutions (1 mg/mL) on freshly cleaved mica, starch chains tended to aggregate to form small particles with average heights of 1.8–5.5 nm, depending on the samples varying in amylose content (Maley et al., 2010). Another study employing a similar preparation method also observed the aggregation of starch chains, probably due to starch retrogradation (Dang et al., 2006). Shorter starch chains tended to aggregate less (An et al., 2011). Molecular combing technique was used to visualise the starch chains (Li et al., 2009). Gelatinized starch in solution that was deposited on the surface of mica was blasted by air for drying, assuming the air-blasting could re-align the molecules to a singular direction (Li et al., 2009). However, the starch chains appeared in the form of bundles, suggesting this method is not efficient to resolve individual chains from each other. By using an aerosol spraying method, individual amylose chains and small amylopectin fibril bundles could be obtained (Maley et al., 2010) (Figure 4). The dispersed amylose chains had an average height of 0.8 nm and a contour length of 140–178 nm, and amylose chains from barley starch with higher amylose content had shorter contour length. All the amylopectin fibril bundles had heights of 1.9–2.9 nm and lengths in µm (Maley et al., 2010). AFM analysis of barley starch showed that genotypes with increasing amylose contents had lower polydispersity index of amylose (Asare et al., 2011). Polydispersity index of amylose was calculated (0.33–1.48) from AFM data, assuming amylose is in the helical form (six sugar residues per turn) and 1.32 Å rise per residue with a linear mass density of 1220

Da/nm. Another method employed surfactant (Tween-20) in hot pea amylose solution to prevent amylose from aggregation by adapting a V-type helix upon cooling (Gunning et al., 2003). Branched amylose chains have been observed (Figure 5). From the distribution of chain lengths and the polydispersity of amylose, the molecular weight was estimated as 1.08×10^6 (Gunning et al., 2003). This is in agreement with the value of 0.84×10^6 which was calculated from light scattering results on pea amylose isolated by the same method (Gunning et al., 2003), confirming the ability of AFM for structural quantification at the molecular level.

Therefore, to be able to accurately quantify the metrics of amylose such as molecular weight by AFM, the biopolymer chains should be dispersed well to prevent any aggregation. It should also be stressed that the nature of the observed chains must be confirmed to exclude any artefact (e.g., by using starch-degrading amylases) (Gunning et al., 2003). For the amylopectin biopolymer chains, the branches are arranged to form clusters. So far, the cluster structure of amylopectin has not been visualized. A method to prevent the molecular aggregation of amylopectin upon starch gelatinization remains to be developed.

Gelatinization and retrogradation

The process of gelatinization and retrogradation of starch has been visualized by AFM (Liu et al., 2005, 2007; Tang & Copeland, 2007). When the maize starch in water was heated, tightly bound and twisted nano-structural units were observed leaching out the granules at specific locations of granules during the initial stage (Liu et al., 2005). These units, coming into contact with water, dispersed. It was neither clear that if these structural units were amylose, amylopectin, or their mixture, nor if they were bundles of starch biopolymer chains. The starch was also gelatinized by

microwaving, and similar phenomenon was observed (Liu et al., 2007). The observed leaching of these units may be related to the amylose leaching during granular swelling (Shi et al., 1991). Amylose plays a major role in the microstructure of gelatinized starch (Tang & Copeland, 2007). Gelatinized wheat starch with an amylose content of 31% or 26% formed an extended network at 90 ^{o}C, while that of 6% amylose content formed no network as observed under AFM (Figure 6). The width of the observed strands in the network suggested that they were likely amylose aggregates rather than single amylose molecules.

Retrogradation

Retrogradation of wheat and maize starches was followed by AFM (Tang & Copeland, 2007). The gelatinized starch with an amylose content of 26% formed an extended network upon cooling to 37 ^{o}C. When the monoglycerides were added to form inclusion complexes with amylose, no extended network was observed. AFM data supported the bulky properties that gel of cooled starch with the extended network was firm, while that without the network was weak and soft. The results confirmed that amylose is critical for the gelation of starch.

Modified starch

Native starches from diverse botanical sources have been modified chemically, physically, or enzymatically to obtain novel properties. The modifications may bring changes to the starch structure, which has been followed by AFM (Table 1).

Chemical modification

Native cassava and maize starches have been subjected to acid hydrolysis (Beninca et al., 2013; Baker et al., 2001). Mild hydrolysis by HCl (0.15 mol/L, 8 h, 30 and 50 ^{o}C) decreased the

surface roughness of cassava starch (Beninca et al., 2013). When using a more concentrated HCl solution (2.5 N, 30 °C for 5 days) to remove the less crystalline and amorphous parts of the granules, blocklets of 10–30 nm in size were exposed (Baker et al., 2001). This size is comparable to that of the nano-structural unit observed on the surface of rice starch that was plasticised and freeze-dried as discussed above (Ayoub et al., 2006). It was suggested that these small-sized blocklets may be related to the amylopectin super helix as proposed previously (Oostergetel & van Bruggen, 1993).

Waxy maize starch in the granular form was modified by octenyl succinate anhydrate (Wetzel et al., 2010). The distribution of the modifying groups may influence the functional properties of the resulting starch. AFM analysis of the surface of modified starch revealed that small particles localised on specific areas of the surface. These particles may be related to the site of modifications.

Physical modification

Heat moisture treatment (HMT)

AFM analysis showed that HMT decreased the occurrence of protrusions and pores, and increased that of round-shaped depressions and small protrusions while enhancing the smoothness of the surface (Jiranuntakul et al., 2013). This may be due to partial gelatinization and retrogradation of the surface, as well as compression of blocklets (Jiranuntakul et al., 2013). The gelatinized layer of starch on the surface during HMT may prevent the water from easy penetration. This may facilitate suitable mobility of starch chain segments with limited amount of water inside the granules.

Deep freezing by liquid nitrogen

The effect of liquid nitrogen freezing on surface structure of starch, revealed by AFM, was much affected by the moisture content of starch (Szymońska et al., 2000; Szymońska et al., 2003). Oven dried starch with very low moisture content appeared to be little susceptible to the impact of deep freezing. Deep freezing of moisturised starch created folded structure on the surface of granules, and may be attributed to the ice formation which mechanically altered the structure. Multiple deep freezing/thawing cycles resulted in well-ordered structure of 30 nm in size which may be related to amylopectin superhelices as proposed previously (Oostergetel & van Bruggen, 1993).

Spherulite formation

Starch spherulites were formed by rapidly cooling down overheated starch solutions (Nordmark & Ziegler, 2002; Ma et al., 2011). The spherulites were produced from high-amylose maize starch solution (10%, w/w). Radially oriented crystalline lamellae and a central hilum were observed (Figure 7). Maize starch was further fractioned into amylose, amylopectin, and intermediate material fractions. The spherulite forming behaviours of these three fractions were explored (Ma et al., 2011). Samples with a higher ratio of linear to branched material better crystallized to form spherulites. Blocklets with a size of 19–26 nm were observed throughout the spherulites. The similarity between spherulites and native starch granules, which was revealed by AFM and corroborated by other methods, suggested that initiation of the biosynthesis of natural starch granules may be rather physical-chemical.

Milling caused damage

Mechanical damage (friction) by milling increased the height of nodules on granule surface (Barrera et al., 2013). The average roughness on the granule surface (R_a) increased by 4 times when the content of damaged starch increased from 4% to 73%. This may be due to the different susceptibility of the hard blocklets and their soft matrix to the friction (Ridout et al., 2003 and 2006).

Combined modification

Waxy maize starch was pre-treated by hydrolysis with glucoamylase of *Aspergillus niger* before treating with sulfuric acid to produce nanoparticles (LeCorre et al., 2012). Enzyme pre-treatment increased the rate of acid hydrolysis. The nanoparticles had an average size of 145 nm as measured by AFM when the hydrolysis extent was 70%, which could be further reduced by prolonged acid hydrolysis.

Starch films and thermoplastics

Starch has great potential to be processed into diverse biodegradable films and thermoplastics for food and medical applications (Rindlav-Westling et al., 2003; Dimantov et al., 2004; Kontturi et al., 2009; Kuutti et al., 1998; Araújo et al., 2010; Thiré et al., 2003). The surface properties and morphology of starch films are crucial for certain applications, and can be explored by AFM quantitatively and qualitatively. Films were made from autoclaved and gelatinized potato amylose, amylopectin, and starch (Rindlav-Westling and Gatenholm, 2003). The surface imaging by AFM showed that amylopectin film was the smoothest with a roughness of 1 nm, followed by amylose film (roughness, 5 nm), and starch film (roughness of 8 nm) (roughness was calculated as the surface elevation values relative to a center plane). This is probably due to the phase

separation of amylose and amylopectin fractions during film formation. Small protein protrusions were present on the film surface due to phase separation as discussed below (Rindlav-Westling and Gatenholm, 2003). AFM analysis of normal maize starch films by phase contrast imaging also revealed that films had smooth and rough domains, probably due to phase separation between glycerol and starch chains as well as the re-orientation of starch chains (Thiré et al., 2003). Another study claimed that film from high amylose maize starch (70% amylose content) was too rough to be imaged by AFM (tapping mode) (Dimantov et al., 2004). This imaging may be achieved by varying the AFM settings. Starch films and thermoplastics go through ageing process and the properties change with time (Kuutti et al., 1998). Freshly prepared films of oat and barley starches by extrusion with glycerol as plasticizers had homogeneous and smooth surfaces. After 5 weeks storage, the film surface became heterogeneous (Figure 8). The ageing phenomenon of starch films may be attributed to phase separation of starch and glycerol, re-crystallization and re-association of starch polymer chains (Kuutti et al., 1998).

Film preparation methods can affect the surface morphology of the films. AFM has been used to study the surface properties of films from cationic starch of varying hydrophobicity on hydrophilic and hydrophobic surfaces as affected by the preparation method (Kontturi et al., 2009). AFM analysis showed that the spin-coated film was rougher than the film deposited by adsorbing in constant coating concentration. The influence of gelatinization processing on film microstructure was also probed by AFM (Thiré et al., 2003). Under shorter heating time (5 min), some starch granules were not completely ruptured. Increasing heating time (90 min) gave films more homogenous surface as all the granules were completely dispersed.

Films made from maize starch and a poly(ethylene-vinyl alcohol) copolymer blend were immersed in human salivary α-amylase solution at 37 ^{o}C up to 90 days (Araújo et al., 2010). AFM analysis qualitatively showed that the surface porosity, pore size, and roughness of the films increased to various extents, much depending on the original structure of the films.

Interactions of starch with other components

Amylose-guest molecule inclusion complex

Amylose can form V-type inclusion complexes with a range of small guest molecules for diverse applications such as controlled releasing and targeted delivery. Amylose biopolymer chains have been complexed with fatty acids (Lalush et al., 2005; Lesmes et al., 2009; Zabar et al., 2010), flavour compounds (Ades et al., 2012), ibuprofen (a commercial anti-inflammatory drug) (Yang et al., 2013), and polystyrene (Kumar et al., 2013), which have been structurally analysed by AFM. It appeared that all the inclusion complexes had a tendency to aggregate to form particles with a heterogeneous size distribution. Potato amylose was complexed with stearic acid by acidification of an alkaline solution. Structural changes were observed after 24 h upon acidification (Zabar et al., 2010). The surface roughness increased from 7.7 nm to 11.5 nm within 24 h upon the acidification, and aggregates of spheroids were formed. Amylose-stearic acid inclusion complex had an apparent diameter of 182 nm and a height of 4 nm (Lesmes et al., 2009). The preparation method had an effect on the structure of the complexes (Lalush et al., 2005). Amylose-conjugated linoleic acid inclusion complexes prepared by co-precipitation from water/DMSO solution were spherical with an average diameter of 150 nm, while those formed from KOH/HCl method were elongated with an average width of 43–160 nm (Lalush et al.,

2005). All the complexes were heterogeneous in structure. Increasing the unsaturation degree of fatty acids led to the formation of larger particles with a wider variation in size (Lesmes et al., 2009). Amylose was complexed with menthone and menthol by acidification method (Ades et al., 2012). The menthone complexes were rod-like with a length of 2.8 µm, a width of 590 nm, and a height of 63 nm. The menthol complexes were also rod-like with a length of 1.12 µm, a width of 299 nm, and a height of 59 nm (Figure 9). The complexes were all heterogeneous in size. Amylose was complexed with ibuprofen by enzymatic polymerization for amylose formation in the presence of ibuprofen (Yang et al., 2013). The resulting complexes were spherical particles with a size ranging from 30 to 80 nm. Amylose−polystyrene complexes were formed by elongating the styrene chains present in the amylose helical cavity through free radical polymerization (Kumar et al., 2013). The resulting complexes tended to aggregate upon formation. Even though the morphology of these complexes can be revealed by AFM, there appears to lack the relationships between the AFM structural data and the functional properties of these inclusion complexes.

Starch granules from potato, maize, and wheat have been exposed to iodine vapour (Waduge et al., 2010; Park et al., 2011). An environmentally controlled chamber has been used to contain the iodine/water vapour. Schematic illustration of the device for *in situ* visualization of starch-iodine vapour interactions by AFM is presented (Figure 10). Starch biopolymer chains, with a size of a few nm, protruding out of the granule surface, have been observed through iodine vapour absorption behaviours of starch (Figure 11). These chains became rigid after the formation of amylose-iodine inclusion complex. The surface roughness of wheat starch granules increased as a result of iodine-starch polymer interactions (Waduge et al., 2013). By using this iodine-based

technique, the difference in the arrangement of blocklets of maize and potato starches has been observed (Figure 12) (Park et al., 2011; Waduge et al., 2013). Potato starch blocklets are more circular, uniform, and compacted, while maize starch blocklets are more irregular and loosely-packed with two size distributions (Figure 12). This technique also revealed that wheat starch of 28 days after anthesis had the longest polymer chains on granule surface, compared with those from 17 and 47 days (Waduge et al., 2010). The role of these tiny protruding starch chains on granule surface in any functional properties of starch remains to be established.

Starch-enzyme interactions

AFM has been used to visualise the real-time process of starch and enzyme interactions (Morris et al., 2005; Thomson et al., 1994). Starch granules were immersed in water, and α-amylase of porcine pancreas was injected for hydrolysis (Thomson et al., 1994). The surface morphology of granules was recorded by AFM in a real-time manner and showed the enlargement of pin-hole on the surface of granules (Thomson et al., 1994). Potato and maize starch granules were subjected to hydrolysis of *Bacillus subtilis* α-amylase at 50 ^{o}C for 60 min (Sujka et al., 2009). AFM images showed that the differential susceptibility to α-amylolysis in different locations of the granule surface (Figure 13). The depressions caused by α-amylase were ~120 nm in diameter, resulting in increased surface roughness (valley and ridge structure). Pores with depth of 41–68 nm were seen on the surface of maize starch granule, but not on that of potato starch. The accuracy of the depth of pores remains to be studied due to the possible limitations in the thickness and length of AFM probe used in the study (Sujka et al., 2009). Indeed, the pores on maize starch granules may penetrate into the central hilum of the granules (Huber and BeMiller, 1997), thus the depth could be much greater than 70 nm.

In vivo degradation of mango starch was monitored by AFM (Simão et al., 2008). 3 days upon harvesting, depressions less than 5 nm deep were seen. The degradation pattern on the granule surface appeared to be similar to that of α-amylolysis (Figure 13), suggesting the role of α-amylase in the initiation of the *in vivo* starch degradation. In general, α-amylase hydrolysis creates "pin-hole" from the top of granule, and the AFM results support the observations by electron microscopy. Furthermore, some details such as the depth of the pin-holes on the surface of granules may only be provided by AFM which may be further related to the kinetics of enzyme hydrolysis.

Amylose biopolymer chains were isolated by the surfactant-mediated procedures (Gunning et al., 2003). Glucoamylase of *Aspergillus niger* was mixed with amylose iodine-Tween 20 solution and incubated at 20 ^{o}C for 1 h before depositing on freshly-cleaved mica for AFM analysis (Morris et al., 2005). The binding between amylose and the enzyme was clearly observed (Figure 14). Glucoamylases of *A. niger* mutants lacking one of the binding domains interacted with amylose molecules differently from that of the wide type. It was suggested that starch binding domain allows glucoamylase to burrow into the end of crystalline amylose helices for the cleavage. This technique remains to be applied to visualise the interactions of amylopectin polymer chains with hydrolytic enzymes such as α-amylase of *Bacillus amyloliquefaciens* which has been used to isolate the clusters (Pérez & Bertoft, 2010).

Starch-biopolymer interactions and phase separation

During food processing and formulation, diverse ingredients are present and interact with each other. When in much diluted solutions, the system tends to stable. In high solid system such as dried films, the molecular interactions between starch and other components such as non-starch

polysaccharide and protein may result in thermodynamic incompatibility and phase separation. This process has been captured by AFM, providing additional data to support the phase separation phenomenon (Quiroga & Bergenståhl, 2007; Ptaszek & Grzesik, 2007; Ptaszek et al., 2009).

Starch-protein interactions

AFM has been used to monitor the phase separation in films of amylopectin and β-lactoglobulin mixtures (Quiroga & Bergenståhl, 2007). Amylopectin and β-lactoglobulin mixtures of different concentrations and compositions were dissolved for mixing and dried for film formation. Higher concentrations of solids led to more phase separation with a sharp boundary (Figure 15). When the amylopectin and β-lactoglobulin ratios were over 1:3, amylopectin became the continuous phase. When the ratios were below 1:6, β-lactoglobulin was continuous. The AFM results were confirmed by TEM data, while the former provided more dimensional information and simpler sample preparation (Quiroga & Bergenståhl, 2007). For example, the shape of the larger domains with a size up to 370 nm in the film of β-lactoglobulin and amylopectin at 1:1 ratio was rounded rather than spherical.

When films were formed from amylose, amylopectin, and starch solutions, small rounded protrusions of 1–4 nm high and 15–35 nm wide were observed (Rindlav-Westling and Gatenholm, 2003). These protrusions could be removed most by phenol but not water, and were believed be the endogenous starch biosynthetic enzymes in nature. The proteins might have thermodynamically separated from the starch phase during the film formation, and migrated onto the film surface.

Starch-non-starch polysaccharide interactions

Starch and non-starch polysaccharides can be mixed to create novel systems with much altered properties (Dimantov et al., 2004; Ptaszek & Grzesik, 2007; Ptaszek et al., 2009). AFM has been used to image the phase separation of maize starch-non-starch polysaccharide gels at various concentration and composition (Figure 16). Increasing hydrocolloid concentration tends to increase the chance of phase separation. Large continuous phase with a dispersed phase entrapped are commonly noted for various starch and polysaccharide mixtures (Figure 16). The phase separation observed by AFM supported the results of relaxation spectrum as analysed through rheological tests (Ptaszek & Grzesik, 2007; Ptaszek et al., 2009). One multimodal peak of relaxation spectra was observed for systems with homogeneous structure and without phase separation. In contrast, a few peaks were noted for systems with heterogeneous structure and phase separation. Therefore, the rheological properties of starch systems may be structurally corroborated by AFM results. Indeed, AFM has been successfully used to interpret the rheology of food polymer systems other than starch at molecular and colloidal levels (Morris et al., 2001). Films of high-amylose maize starch and pectin mixtures at different ratios were formed by drying solutions (Dimantov et al., 2004). Two distinct regions characteristic to pectin and starch, respectively, were detected by AFM, indicating the phase separation during film formation. The roughness of starch films was decreased by pectin addition. This result from AFM analysis contradicted with the other report on starch-pectin films which was suggested to be highly compatible composites studied by techniques (including scanning electron microscopy) other than AFM (Fishman et al., 1996). This may suggest that AFM can be a powerful tool to detect the microstructure of films which could not be probed by other types of microscopy.

AFM-based force spectroscopy

At a specific image point, variations in the tip-sample separation can be employed to generate a force–distance curve (Butt et al., 2005). Through the modification of the surface of probe/sample, AFM can be used to quantify the interactive forces at a single molecular level (force spectroscopy) (Butt et al., 2005; Morris et al., 2011). The elasticity of certain types of polysaccharides is determined by force-induced conformational transitions of the pyranose ring. Force–extension spectrum is dependent on the ground-energy conformation of the pyranose ring and the type of glycosidic linkages (Marszalek et al., 2001). AFM-based force spectroscopy has been successfully used to differentiate starch molecules (amylopectin) from other non-starch polysaccharides (agarose and λ-carrageenan) of algae on single-molecular level in a solution of polysaccharide mixtures (Marszalek et al., 2001). Drawbacks of this type of analytical techniques are the low efficiency (10%) and lack of quantitative basis. Nevertheless, it is tempting to suggest that this technique may be further developed to differentiate various types of starch biopolymer chains with different branching pattern and chain length on a single-molecule level.

AFM-based force spectroscopy has been used to detect the formation of V-type amylose inclusion complexes with iodine and butanol in solution (Zhang et al., 2006). Using AFM, individual amylose chains were forced to be adsorbed to a surface to enter the solvents to overcome the precipitation tendency of the resulting complexes. Stretch-release measurements of the amylose-guest molecule interactions were thus allowed to be conducted in solution. The formation of individual amylose helices induced by butanol and iodine were quantified. Amylose

helices with iodine extended and relaxed more easily than those with butanol in solution. The pitch of the helix was 1.3 Å/ring and the force for the formation of the helix was 50 pN in solution. The data agreed well with that of wide-angle X-ray diffractometry. This technique may complement other techniques to study the starch-guest molecule interactions in solution. As discussed above, diverse guest molecule-amylose inclusion complexes vary in shape and size upon precipitation. AFM-based force spectroscopy may provide some insights into this diversity, which remains to be studied.

AFM-based force spectroscopy has been used to probe the surface adhesion properties of wheat flour components (including starch granules) against glass and polysine surfaces (Duri et al., 2013) (Figure 17). Weibull analysis was conducted to quantify the degree of hydrophobic interactions. It was found that starch and arabinoxylan had fewer interactions than protein with the two surfaces. The interactions between starch and other food components (instead of glass and polysine) can be further explored to provide structural basis for processing such as mixing. It remains to be studied if this can also differentiate starch types as each type of starch tends to vary in the surface morphology.

Conclusions

AFM has been used to image starch and diverse starch mixtures in their native states as well as during processing and interaction. Blocklet structures on the surface of and also within the crystalline and amorphous lamellae of starch granules were imaged. On the molecular level, the single amylose chains were observed. During starch gelatinization, chain bundles leached out of the granules. Upon retrogradation, starch with higher amylose content formed an extended

network while waxy starch showed aggregates. Structural changes of starch upon modifications and film formation, as well as the interactions of starch with iodine, enzymes and proteins, fatty acids, flavour compounds, and non-starch polysaccharides have been monitored, providing support for the resulting macroscopic properties. AFM-based force microscopy provided information on elasticity and adhesion properties of starch.

Sample preparation method appears to be rather critical for obtaining the correct images and subsequent data interpretation. Preparation method to visualize the cluster structure of amylopectin remains to be developed. In some starch systems such as V-type amylose-complexes, the correlations between the structural features of AFM and the bulky physicochemical properties remain to be established. Quantitative analysis by AFM force spectroscopy can be better exploited to improve the efficiency of analysis, especially in the wet starch systems, and to relate the AFM results to that of other analytical techniques.

References

Ades, H., Kesselman, E., Ungar, Y., and Shimoni, E. (2012). Complexation with starch for encapsulation and controlled release of menthone and menthol. *LWT-Food Sci. Technol.* **45**:277–288.

An, H., Liang, H., Liu, Z., Yang, H., Liu, Q., and Wang, H. (2011). Nano-structures of debranched potato starch obtained by isoamylolysis. *J. Food Sci.* **76**:N11–N14.

Araújo, M. A., Cunha, A. M., and Mota, M. (2010). Changes on surface morphology of corn starch blend films. *J. Biomed. Mater. Res. A.* **94A**:720–729.

Asare, E. K., Jaiswal, S., Maley, J., Båga, M., Sammynaiken, R., Rossnagel, B. G., and Chibbar, R. N. (2011). Barley grain constituents, starch composition, and structure affect starch in vitro enzymatic hydrolysis. *J. Agric. Food Chem.* **59**:4743–4754.

Ayoub, A., Ohtani, T., and Sugiyama, S. (2006). Atomic force microscopy investigation of disorder process on rice starch granule surface. *Starch/Stärke* **58**:475–479.

Baker, A. A., Miles, M. J., and Helbert, W. (2001). Internal structure of the starch granule revealed by AFM. *Carbohydr. Res.* **330**:249–256.

Baldwin, P. M., Adler, J., Davies, M. C., and Melia, C. D. (1998). High resolution imaging of starch granule surfaces by atomic force microscopy. *J. Cereal Sci.* **27**:255–265.

Barrera, G. N., Calderón-Domínguez, G., Chanona-Pérez, J., Gutiérrez-López, G. F., Leóna, A. E., and Ribotta, P. D. (2013). Evaluation of the mechanical damage on wheat starch granules by SEM, ESEM, AFM and texture image analysis. *Carbohydr. Polym.* **98**:1449–1457.

BeMiller, J., and Whistler, R. (2009). *Starch: Chemistry and Technology*. Academic Press.

Beninca, C., Colman, T. A. D., Lacerda, L. G., Filho, M. A. S. C., Bannach, G., and Schnitzler, E. (2013). The thermal, rheological and structural properties of cassava starch granules modified with hydrochloric acid at different temperatures. *Thermochim. Acta* **552**:65–69.

Binnig, G., Quate, C. F., and Gerber, C. (1986). Atomic force microscope. *Phys. Rev. Lett.* **56**:930–933.

Butt, H. J., Cappella, B., and Kappl, M. (2005). Force measurements with the atomic force microscope: Technique, interpretation and applications. *Surf. Sci. Rep.* **59**:1–152.

Cabálková, J., Pøibyl, J., Skládal, P., Kulich, P., and Chmelik, J. Size, shape and surface morphology of starch granules from Norway spruce needles revealed by transmission electron microscopy and atomic force microscopy: effects of elevated CO_2 concentration. *Tree Physiol.* **28**:1593–1599.

Dang, J. M. C., Braet, F., and Copeland, L. (2006). Nanostructural analysis of starch components by atomic force microscopy. *J. Microsc.* **224**:181–186.

Dimantov, A., Kesselman, E., and Shimoni, E. (2004). Surface characterization and dissolution properties of high amylose corn starch–pectin coatings. *Food Hydrocolloids* **18**:29–37.

Duri, A., George, M., Saad, M., Gastaldi, E., Ramonda, M., and Cuq, B. (2013). Adhesion properties of wheat-based particles. *J. Cereal Sci.* **58**:96–103.

Fishman, M. L., Coffin, D. R., Unruh, J. J., and Ly, T. (1996). Pectin/starch/glycerol films: Blends or composites? *J. Macromol. Sci. Pure Appl. Chem.* **33**:639–654.

Gallant, D. J., Bouchet, B., and Baldwin, P. M. (1997). Microscopy of starch: evidence of a new level of granule organization. *Carbohydr. Polym.* **32**:77–191.

Gunning, A. P., Giardina, T. P., Faulds, C. B., Juge, N., Ring, S. G., Williamson, G., and Morris, V. J. (2003). Surfactant-mediated solubilisation of amylose and visualisation by atomic force microscopy. *Carbohydr. Polym.* **51**:177–182.

Huber, K. C., and BeMiller, J. N. (1997). Visualization of channels and cavities of corn and sorghum starch granules. *Cereal Chem.* **74**:537–541.

Jiranuntakul, W., Sugiyama, S., Tsukamoto, K., Puttanlek, C., Rungsardthong, V., Puncha-Arnon, S., and Uttapap, D. (2013). Nano-structure of heat–moisture treated waxy and normal starches. *Carbohydr. Polym.* **97**:1–8.

Kontturi, K. S., Holappa, S., Kontturi, E., Johansson, L. S., Hyvärinen, S., Peltonen, S., and Laine, J. (2009). Arrangements of cationic starch of varying hydrophobicity on hydrophilic and hydrophobic surfaces. *J. Colloid Interface Sci.* **336**:21–29.

Kumar, K., Woortman, A. J. J., and Loos, K. (2013). Synthesis of amylose−polystyrene inclusion complexes by a facile preparation route. *Biomacromolecules* **14**:1955−1960.

Kuutti, L., Peltonen, J., Myllärinen, P., Teleman, O., and Forssell, P. (1998). AFM in studies of thermoplastic starches during ageing. *Carbohydr. Polym.* **37**:7–12.

Lalush, I., Bar, H., Zakaria, I., Eichler, S., and Shimoni, E. (2005). Utilization of amylose-lipid complexes as molecular nanocapsules for conjugated linoleic acid. *Biomacromolecules* **6**:121–130.

LeCorre, D., Vahanian, E., Dufresne, A., and Bras, J. (2012). Enzymatic pretreatment for preparing starch nanocrystals. *Biomacromolecules* **13**:132−137.

Lesmes, U., Cohen, S. H., Shener, Y., and Shimoni, E. (2009). Effects of long chain fatty acid unsaturation on the structure and controlled release properties of amylose complexes. *Food Hydrocolloids* **23**:667–675.

Li, H., Liu, Z. D., Liu, B.,, Chen, J. H., Sun, Y. N., Lv, X. L., Zhang, Z. S., Sun, P., Zhang P., and Wang, Y. L. (2009). Application of the molecular combing technique to starch granules. *Molecules* **14**:4079–4086.

Liu Z., Liu, P., and Kennedy, J. F. (2005). The technology of molecular manipulation and modification assisted by microwaves as applied to starch granules. *Carbohydr. Polym.* **61**:374–378.

Liu, P., Chen, L., Corrigan, P. A., Yu, L., and Liu, Z. (2008). Application of atomic force microscopy on studying micro- and nano-structures of starch. *Int. J. Food Eng.* **4**:8.

Ma, U. V. L., Floros, J. D., and Ziegler, G. R. (2011). Effect of starch fractions on spherulite formation and microstructure. *Carbohydr. Polym.* **83**:1757–1765.

Maley, J., Asare, E. K., Båga, M., Rossnagel, B. G., Chibbar, R. N., and Sammynaiken, R. (2010). Application of aerosol-spray deposition for determination of fine structure of barley starch using atomic force microscopy. *Starch/Stärke* **62**:676–685.

Marszalek, P. E., Li, H., and Fernandez, J. M. (2001). Fingerprinting polysaccharides with single molecule atomic force microscopy. *Nature Biotechnol.* **19**:258–262.

Morris, V. J., Gunning, A. P., Faulds, C. B., Williamson, G., and Svensson, B. (2005). AFM images of complexes between amylose and *Aspergillus niger* glucoamylase mutants, native and mutant starch binding domains: A model for the action of glucoamylase. *Starch/Stärke* 57:1–7.

Morris, V. J., Kirby, A. R., and Gunning, A. P. (2010). *Atomic force microscopy for biologists*. London : Imperial College Press.

Morris, V. J., Woodward, N. C., and Gunning, A. P. (2011). Atomic force microscopy as a nanoscience tool in rational food design. *J. Sci. Food Agric.* **91**:2117–2125.

Neethirajan, S., Thomson, D. J., Jayas, D. S., and White, N. D. G. (2008). Characterization of the surface morphology of durum wheat starch granules using atomic force microscopy. *Microsc. Res. Tech.* **71**:125–132.

Nordmark, T. S., and Ziegler, G. R. (2002). Structural features of non-granular spherulitic maize starch. *Carbohydr. Res.* **337**:1467–1475.

Ohtani, T., Yoshino, T., Hagiwara, S., and Maekawa, T. (2000). High-resolution imaging of starch granule structure using atomic force microscopy. *Starch/Stärke* **52**:150–153.

Oostergetel, G. T., and van Bruggen, E. F. J. (1993). The crystalline domains in potato starch granules are arranged in a helical fashion. *Carbohydr. Polym.* **21**:7–12.

Park, H., Xu, S., and Seetharaman, K. (2011). A novel in situ atomic force microscopy imaging technique to probe surface morphological features of starch granules. *Carbohydr. Res.* 346:847–853.

Parker, M. L., Kirby, A. R., and Morris, V. J. (2008). *In situ* imaging of pea starch in seeds. *Food Biophys* **3**:66–76.

Pérez, S., and Bertoft, E. (2010). The molecular structures of starch components and their contribution to the architecture of starch granules: A comprehensive review. *Starch/Stärke*, **62**:389–420.

Ptaszek, A., Berski, W., Ptaszek, P., Witczak, T., Repelewicz, U., and Grzesik, M. (2009). Viscoelastic properties of waxy maize starch and selected non-starch hydrocolloids gels. *Carbohydr. Polym.* **76**:567–577.

Ptaszek, P., and Grzesik, M. (2007). Viscoelastic properties of maize starch and guar gum gels. *J. Food Eng.* **82**:227–237.

Quiroga, C. C., and Bergenståhl, B. (2007). Characterization of the microstructure of phase segregated amylopectin and β-lactoglobulin dry mixtures. *Food Biophys.* **2**:172–182.

Ridout, M. J., Parker, M. L., Hedley, C. L., Bogracheva, T. Y., and Morris, V. J. (2004). Atomic force microscopy of pea starch: Origins of image contrast. *Biomacromolecules* **5**:1519–1527.

Ridout, M.J., Parker, M. L., Hedley, C. L., Bogracheva, T.Y., and Morris, V. J. (2003). Atomic force microscopy of pea starch granules: granule architecture of wild-type parent, *r* and *rb* single mutants, and the *rrb* double mutant. *Carbohydr. Res.* **338**:2135–2147.

Ridout, M.J., Parker, M. L., Hedley, C. L., Bogracheva, T.Y., and Morris, V. J. (2006). Atomic force microscopy of pea starch: Granule architecture of the *rug3-a*, *rug4-b*, *rug5-a* and *lam-c* mutants. *Carbohydr. Polym.* **65**:64–74.

Rindlav-Westling, Å., and Gatenholm, P. (2003). Surface composition and morphology of starch, amylose, and amylopectin films. *Biomacromolecules* **4**:166–172.

Shi, Y. C., Seib, P. A. and Lu, S. P. W. (1991). Leaching of amylose from wheat and corn starch. *Water Relationships in Foods*, Levine, H. and Slade, L. (Eds) pp.667–686. Springer.

Simão, R. A., Silva, A. P. F. B., Peroni, F. H. G., Nascimento, J. R. O. D., Louro, R. P., Lajolo, F. M., and Cordenunsi, B. R. (2008). Mango starch degradation. I. A microscopic view of the granule during ripening. *J. Agric. Food Chem.* **56**:7410–7415.

Sujka, M., and Jamroz, J. (2009). α-Amylolysis of native potato and corn starches – SEM, AFM, nitrogen and iodine sorption investigations. *LWT-Food Sci. Technol.* 42:1219–1224.

Szymońska, J., Krok, F., and Tomasik, P. (2000). Deep-freezing of potato starch. *Int. J. Biol. Macromol*. **27**:307–314.

Szymońska, J., Krok, F., Komorowska-Czepirska, E., and Rębilas, K. (2003). Modification of granular potato starch by multiple deep-freezing and thawing. *Carbohydr. Polym.* **52**:1–10.

Tang, M. C., and Copeland, L. (2007). Investigation of starch retrogradation using atomic force microscopy. *Carbohydr. Polym.* **70**:1–7.

Thiré, R. M. S. M., Simão, R. A., and Andrade, C. T. (2003). High resolution imaging of the microstructure of maize starch films. *Carbohydr. Polym.* **54**:149–158.

Thomson, N. H., Miles, M. J., Wills, H. H., Ring, S. G., Shewry, P. R., and Tatham, A. S. (1994). Real-time imaging of enzymatic degradation of starch granules by atomic force microscopy. *J. Vac. Sci. Technol. B*. **12**:1565–1568.

Tsukamoto, K., Ohtani, T., and Sugiyama, S. (2012). Effect of sectioning and water on resin-embedded sections of corn starch granules to analyze inner structure. *Carbohydr. Polym.* **89**:1138–1149.

Waduge, R. N., Xu, S., and Seetharaman, K. (2010). Iodine absorption properties and its effect on the crystallinity of developing wheat starch granules. *Carbohydr. Polym*. **82**:786–794.

Waduge, R. N., Xu, S., Bertoft, E., and Seetharaman, K. (2013). Exploring the surface morphology of developing wheat starch granules by using atomic force microscopy. *Starch/Stärke* **65**:398–409.

Wetzel, D. L., Shi, Y. C., and Schmidt, U. (2010). Confocal Raman and AFM imaging of individual granules of octenyl succinate modified and natural waxy maize starch. *Vib. Spectrosc.* **53**:173–177.

Yang, L., Zhang, B., Yi, J., Liang, J., Liu, Y., and Zhang, L. M. (2013). Preparation, characterization, and properties of amylose-ibuprofen inclusion complexes. *Starch/Stärke* **65**:593–602.

Zabar, S., Lesmes, U., Katz, I., Shimoni, E., and Bianco-Peled, H. (2010). Structural characterization of amylose-long chain fatty acid complexes produced via the acidification method. *Food Hydrocolloids* **24**:347–357.

Zhang, Q., Lu, Z., Hu, H., Yang, W., and Marszalek, P. E. (2006). Direct detection of the formation of V-amylose helix by single molecule force spectroscopy. *J. Am. Chem. Soc.* **128**:9387–9393.

Table 1 Applications of AFM in diverse starch systems

Target	Starch type	Experiments	Imaging mode	Major findings	References
Surface morphology	Potato, maize	Starch interaction with iodine and water vapours	Tapping	Hair-like structures with a size of 1.5 nm were observed on the surface. The distribution of these structures depends on structure and organization of blocklets on granule surface	Park et al., 2011
Surface morphology	Rice	Starch was subjected to plasticizing by water and lyophilization	Tapping	Plasticizing/lyophilization reduced the size of nodule structures on granule surface from 60–80 nm to 20–40 nm	Ayoub et al., 2006
Surface morphology	Potato	Potato starch granules were oven-	Non-contact	Different drying processes greatly	Szymońska et al.,

		dried, air-dried, and moisturised before deep-freezing		influenced the surface morphology of granules	2000
Surface morphology	Wheat	Mechanical damage (milling) was made on starch granules	Tapping	Mechanical damage increased the height of nodules	Barrera et al., 2013
Surface morphology	Wheat	Starch granules from hard red spring wheat collected at 7–49 days after anthesis (DAA) were imaged	Tapping, non-contact	Starch of 7 DAA had a mono-modal size distribution. Fuzzy and large blocklets observed at early DAA became smaller and less fuzzy towards maturity. Starch of 28 DAA had the longest polymer chains protruding from the granule surface to interact with iodine	Waduge et al., 2010 and 2013
Surface morphology	Potato, wheat		Constant contact	Potato starch had more protrusions than	Baldwin et al.,

			force	wheat starch on a flatter surface. Protrusions were 50–300 nm in diameter, and the surface was made of structural units of 10–50 nm in size	1998
Surface morphology	Mango	Starch degradation was monitored *in vivo*	Intermittent contact	Depressions on the surface of granules were formed during degradation and were attributed to α-amylolysis	Simão et al., 2008
Surface morphology	Rice, maize, potato	Starch with a moisture content of 25% was treated at 100 ^{o}C for 16 h	Intermittent contact	HMT increased the surface smoothness and decreased the size of protrusions	Jiranuntakul et al., 2013
Surface morphology	Cassava	Starch was treated with HCl solution	Non-contact	Acid hydrolysis increased the smoothness of the surface of granules	Beninca et al., 2013

Surface morphology	Potato, oat, cassava, wheat, barley, maize,		Non-contact	Cassava starch had smoother surface than potato starch. Blocklet structure was observed on all starch surfaces	Juszczak et al., 2003a and 2003b
Surface morphology	Potato	Freeze-thaw	Non-contact	Results supported the blocklet model of starch granules	Szymońska & Krok, 2003
Surface morphology	Norway spruce needles		Semi-contact	Granules had fine (protrusions and furrows) and rough (nodules (100 nm in diameter) and grooves (100–500 nm deep) portions of surface	Cabálková et al., 2008

Internal granule morphology	Pea	Starches from pea mutants were sectioned by an ultramicrotome	Contact	The structure of the inner part of granules was heterogeneous. Contrast in the AFM images was attributed to differential water absorption localized in exposed sessions of granules. Growth ring structure under AFM may be visible or not, depending on the amount and presence of amylose in starches from specific pea mutants	Ridout et al., 2003; 2004; 2006
Internal granule morphology	Maize	Starch was embedded in resin and sectioned by microtoming	Tapping and contact	Blocklets within the growth rings of lintnerised starch granules were ~10–30 nm in size	Baker et al., 2001
Internal	Pea	Starch was imaged	Contact	Granules have	Parker et

granule morphology		*in situ* in dried pea seeds		alternating layers with various degrees of crystallinity (instead of the alternating amorphous and crystalline layers)	al., 2008
Internal granule morphology	Maize	Starch was sectioned by an ultramicrotome	Intermitte nt contact	Nanoparticles with a width of ~30 nm and a height of a few nm were observed	Tsukamot o et al., 2012
Surface and internal granule morphology	Durum wheat	Starches of vitreous and nonvitreous durum wheat kernels were compared. Microtomed starch was treated by UV/ozone	Contact	UV/ozone treatment improved the viewing of growth ring structure. Growth rings were observed in the nonvitreous starch granules but not vitreous ones. Nonvitreous durum wheat starch has more amylopectin	Neethiraja n et al., et al., 2008

				molecules than amylose	
Surface and internal granule morphology	Maize, potato, rice, sweet potato, wheat	Sectioning by a microtome, glucoamylase degradation, and physical destruction by a glass homogenizer were employed to exposed the inner part of granules	Contact	Physical destruction was the most effective for imaging inner structure of granules. Particles with a size of 30 nm were seen on all starch granules	Ohtani et al., 2000
Starch retrogradation	Wheat, maize	Retrogradation of starch with different amylose contents	Tapping	An extended network of gelatinized starch formed in the presence of amylose. Aggregates of gelatinized starch formed in the absence of amylose or when the amylose was complexed with guest	Tang & Copeland, 2007

				molecules	
Starch polymer chains	Barley	Aerosol-spray deposition of gelatinized starch was used to prepare samples	Intermittent contact	Aerosol spray deposition could be used to image individual chains of amylose and fibril bundles of amylopectin. Amylose had a length of 178–127 nm and a height of 0.8–0.2 nm. Heights of bundles of amylopectin were 1.9–2.9 nm and lengths were in µm. Polydispersity indexes of amyloses from genotypes with reduced amylose contents were lower than those of genotypes with	Maley et al., 2010; Asare et al., 2011

				higher amylose contents	
Starch polymer chains	Maize	Starch was gelatinized. Samples were prepared by drying a starch solution on a mica surface using a blast of air	Tapping	Starch chains leaching out of granules during gelatinization were observed. Starch chains dispersed from gelatinization were in the form of bundles	Li et al., 2009
Starch polymer chains	Rice and potato	Starch was gelatinized	Non-contact	DP of amyloses of rice and potato starches were quantified by AFM as 1860 and 1440, respectively	Dang et al., 2006
Starch polymer chains	Potato	Potato starch was debranched and further fractionated by gel permeation chromatography	Tapping	A large proportion of chain bundles was 100 nm long, and larger chains appeared to aggregate easily	An et al., 2011

Starch polymer chains	Pea	Amylose was extracted from pea starch by using surfactant (Tween-20) to prevent aggregation	Constant force	Amylose chains and chains with a small number of branches were observed	Gunning et al., 2003
Surface morphology	Maize	Maize starch octenyl succinate was prepared	Non-contact	The modification occurred specifically on certain locations of the granule surface	Wetzel et al., 2010
Starch spherulites	Maize	Spherulites were formed from gelatinized high-amylose starch by heating and cooling a starch solution. The starch was also fractionated to prepare spherulites	Tapping	Blocklets of the spherulites formed from rapid cooling of heated starch solution had a size of 19–26 nm. Central helium and radial orientation of the lamellae-type structures were seen	Ma et al., 2011; Nordmark & Ziegler, 2002
Starch nanoparticles	Maize	Waxy maize starch was hydrolysed by sulfuric acid after	Tapping and conductiv	The resulting nanoparticles had a size of ~68 nm	LeCorre et al., 2012

		enzymatic treatment for starch nanoparticle production	e		
V-type amylose inclusion complex	Maize	Amylose formed inclusion complexes with menthone and menthol through KOH/HCl method for controlled releasing properties	Contact and intermittent contact	Complexes were rod-like. The length, width, and height of menthone-amylose complexes were 2.8 µm, 590 nm, and 63 nm, respectively. Those of menthol complexes were 1.1 µm, 299 nm, and 59 nm, respectively	Ades et al., 2012
	Potato amylose	Stearic acid, *cis*-9-octadecenoic acid, *cis*-9,*cis*-12-octadecadienoic acid	Contact	Increasing unsaturation of fatty acids resulted in the formation of more dispersed and larger particles. Amylose-stearic acid	Lesmes et al., 2009

				complexes had an a diameter of 182 nm and a height of 4 nm	
	Potato and synthetic amylose	Amylose-ibuprofen complexes were prepared by enzymatic synthesis of amylose and by acidification of an alkali solution	Tapping	The complexes aggregated to form spherical particles of 30 to 80 nm in size	Yang et al., 2013
	Potato amylose	A range of long chain fatty acids formed inclusion complexes with amylose through acidification method	Contact	Surface roughness increased during formation of V-type complex. The complexes aggregated to form spheroids	Zabar et al., 2010
	n.a.	Amylose−polystyrene inclusion complexes were prepared by first	Tapping	The complexes tended to aggregate	Kumar et al., 2013

		inserting styrene in amylose helical cavity before free radical polymerization of styrene			
	Potato	Single-walled carbon nanotube interacted with amylose	n.a.	Small nanotubes formed inclusion complexes with amylose	Lii et al., 2003a and 2003b
Film	Barley and oat	Changes in surface morphology of thermoplastic starch (TPS) films with water and glycerol prepared by extrusion during ageing were noted	Constant force and friction modes	The surface of fresh films was flat and homogeneous. Ageing imparted roughness and heterogeneity to film surface, which was attributed to starch–glycerol phase separation and starch re-crystallization	Kuutti et al., 1998

Film	Potato	Acetylated and cationic starch was deposited by spin coating or adsorbing on hydrophilized and hydrophobized silica surfaces to form films	Tapping	Films by spin coating were rougher than those by adsorbing	Kontturi et al., 2009
Film	Maize	Films of starch and a poly(ethylene-vinyl alcohol) copolymer were hydrolysed by human salivary α-amylase at 37 ^{o}C	Tapping	α-Amylolysis increased the roughness of the surface while creating small pits	Araújo et al., 2010
Film	Maize	Starch films were prepared by heating starch and glycerol mixtures for various length before casting	Intermitte nt contact	Smooth and rough structures were separated by depression or nodules on film surface. The surface morphology depends on the	Thiré et al., 2003

				preparation conditions	
Film	High amylose maize	High amylose maize-pectin films were formed. The films were subjected to dissolution and enzymatic hydrolysis analysis	Tapping	Roughness of film surface increased with increasing maize starch content	Dimantov et al., 2004
Film	Potato	Potato amylose, amylopectin, and starch were made into films	Tapping	Amylose film was rougher than amylopectin film. Small rounded protrusions of a of 15–35 nm wide and 1–4 nm high were observed	Rindlav-Westling & Gatenholm, 2003
Interactions with glucoamyla	Pea	Binding of glucoamylases from *Aspergillus niger*	Constant force	Starch binding domains of the glucoamylase were	Morris et al., 2005

ses		(including mutants) with amylose was visualised		visualised as a template for an expanded amylose double helix to bind onto. A proposal on how the glucoamylase could act on the crystalline starch was suggested	
Interactions with α-amylase	Wheat	Starch was degraded by α-amylase	Contact	α-Amylase created a "pin-hole" in granule surface	Thomson et al., 1994
Surface morphology of starch during α-amylolysis	Potato and maize	Starch was hydrolysed by α-amylase of *Bacillus subtilis* (50 ^{o}C up to 60 min)	Tapping	Depressions with a size of ~121 nm in diameter were observed on the surface of starch due to α-amylolysis while the blocklets of ~20 nm in diameter became more obvious	Sujka & Jamroz, 2009
Starch-non-	Maize	Maize starch and	Contact	Surface of the gels	Ptaszek et

starch polysaccharide interaction		non-starch polysaccharides (guar gum, carboxymethylcellulose, and xanthan gum) mixtures were subjected to gelation		was imaged by AFM. The surface of gel was homogeneous and heterogeneous, depending on the composition of the polysaccharides	al., 2007 & 2009
Starch-protein interaction	Waxy maize	Amylopectin and β-lactoglobulin blends in solution with different concentration and composition were dried	Tapping	Surface morphology of the mixtures was monitored by AFM. Phase separation occurred at certain ratios of these two components with higher concentrations	Quiroga & Bergenstål hl, 2007

Intermittent contact mode is also called tapping mode; n.a., not available

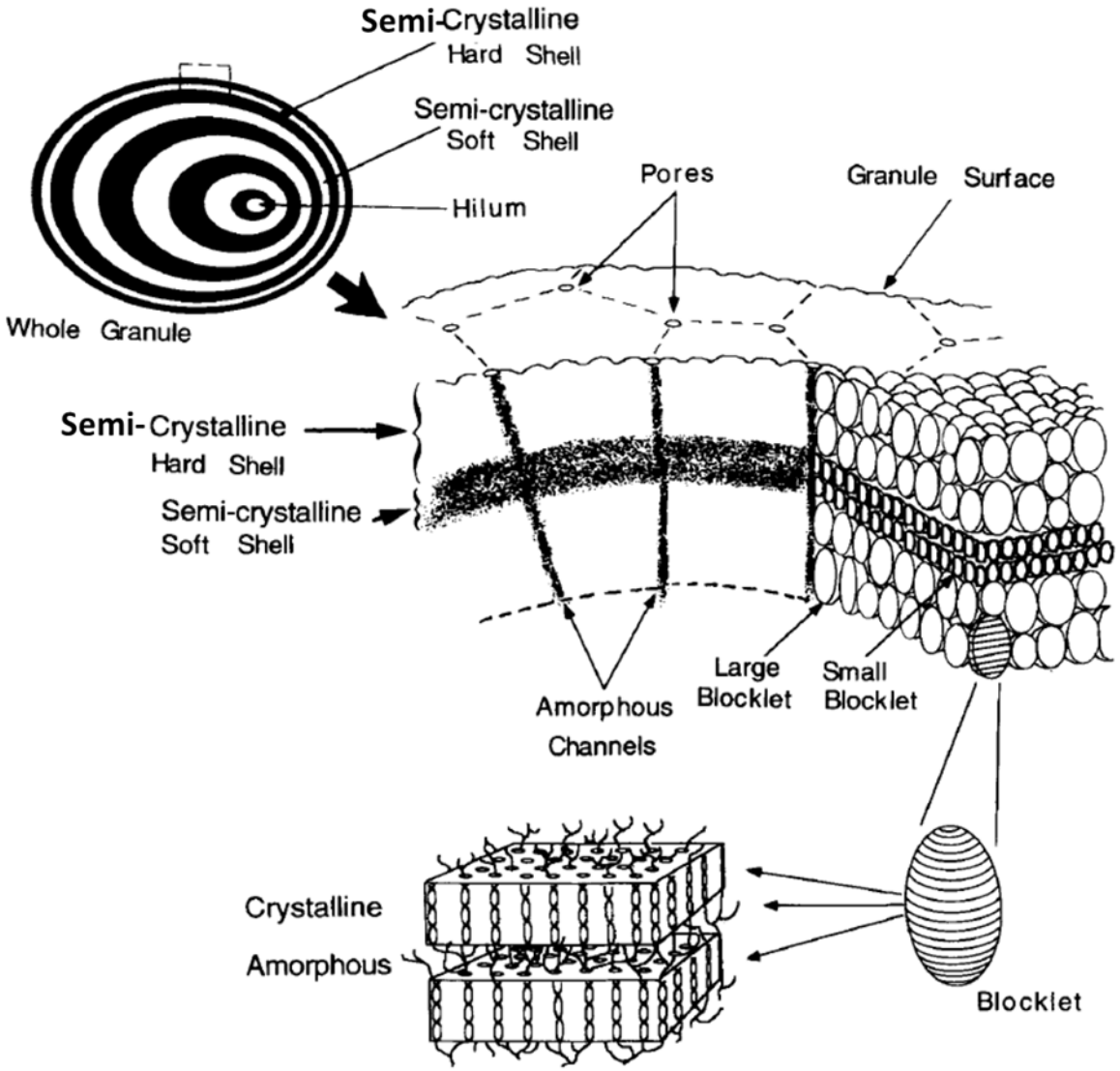

Figure 1. Schematic illustration of diverse structural levels of starch granule (Gallant et al., 1997)

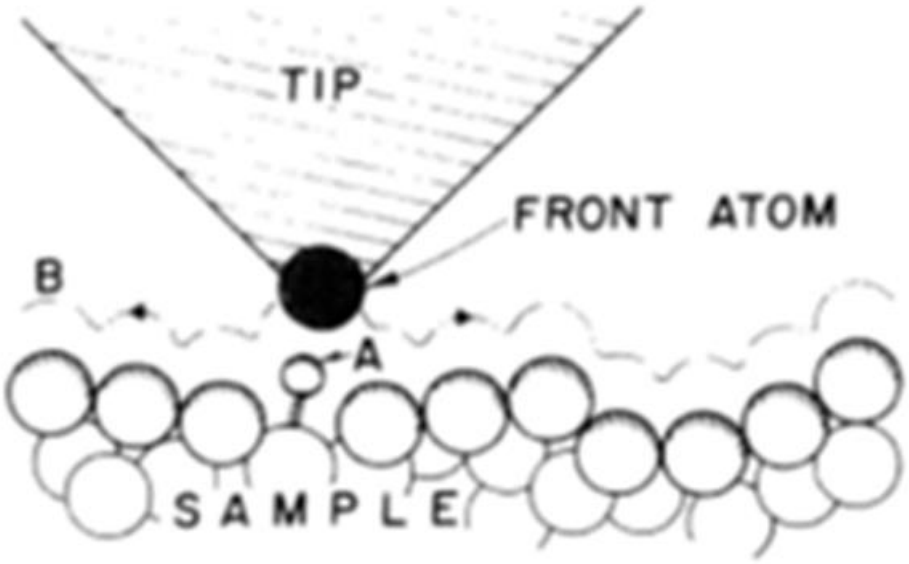

Figure 2. Schematic illustration of operation principles of AFM. The probing tip follows contour B of the sample (Binnig et al., 1986)

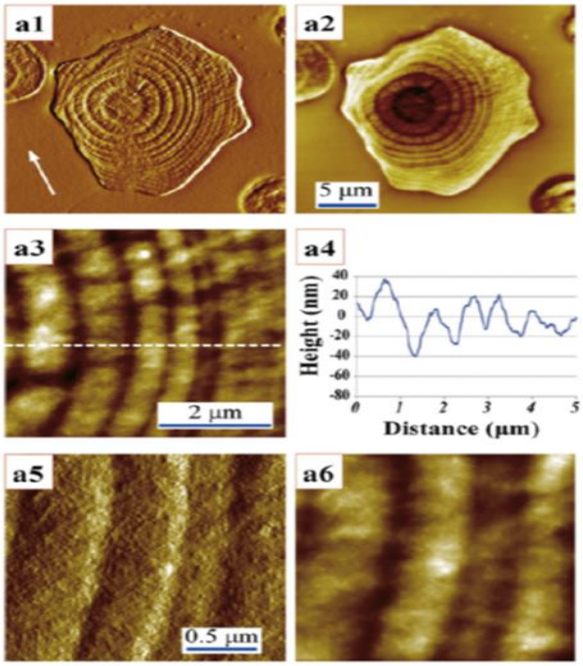

Figure 3. AFM images of sectioned maize starch granules. a1 and a2, error signal and height images of complete granule, arrow indicates the sectioning direction; a3, height image of a magnified section of (a2); a4, height distribution of cross section along the dashed line of a3; a5 and a6, error signal and height image of a further magnified section (Tsukamoto et al., 2012)

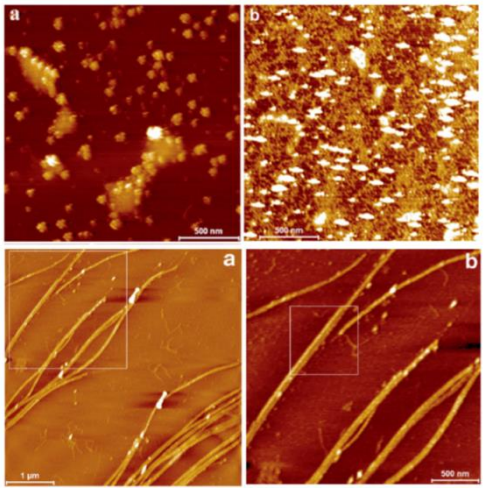

Figure 4. AFM topography images of gelatinized barley starch deposited on mica using drop (top a and b) and aerosol (bottom a and b) deposition methods. a, waxy barley; b, barley starch with 26% amylose (Maley et al., 2010)

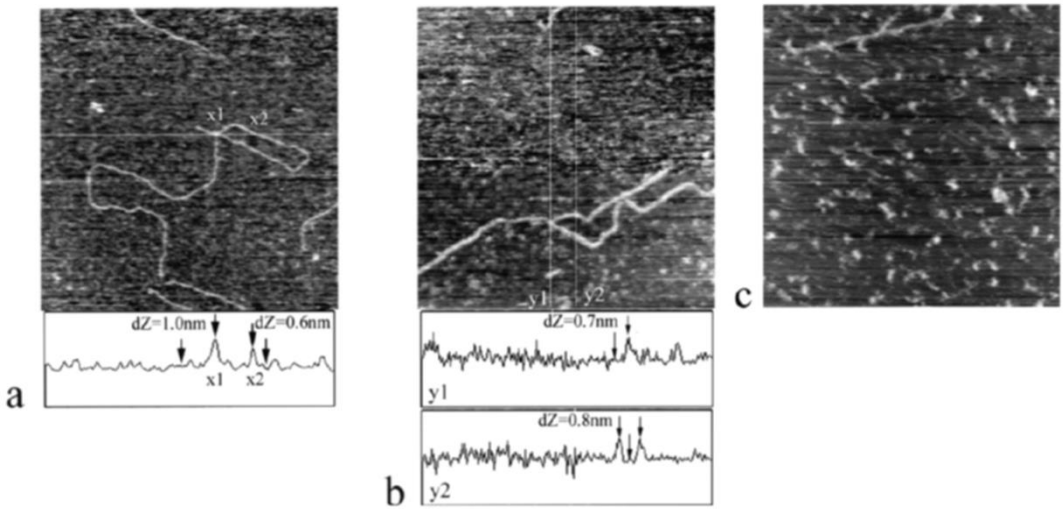

Figure 5**.** AFM image of pea amylose prepared by surfactant-mediated solubilisation. (a) Amylose molecules overlapping; (b) branched amylose with a longer branch chain; (c) branched amylose with a shorter branch chain. dZ, height (Gunning et al., 2003)

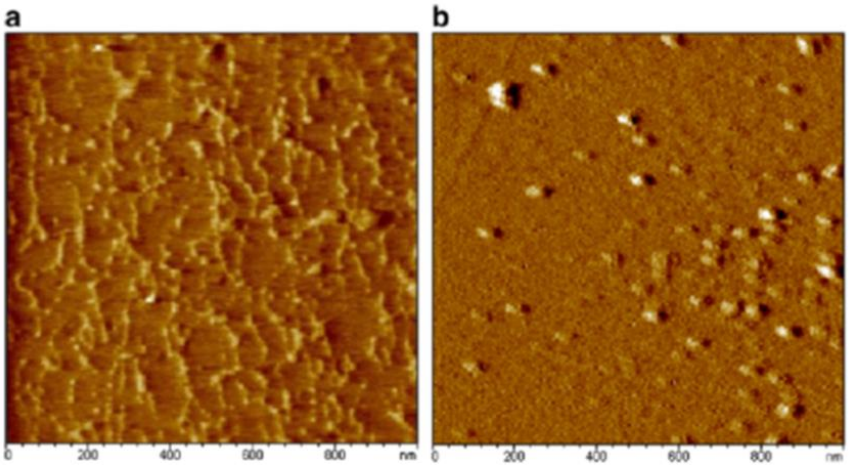

Figure 6. AFM image of gelatinized maize starches with amylose content of 31% (a) and 7% (b). The temperature of samples during the imaging was 90 ^{o}C (Tang & Copeland, 2007)

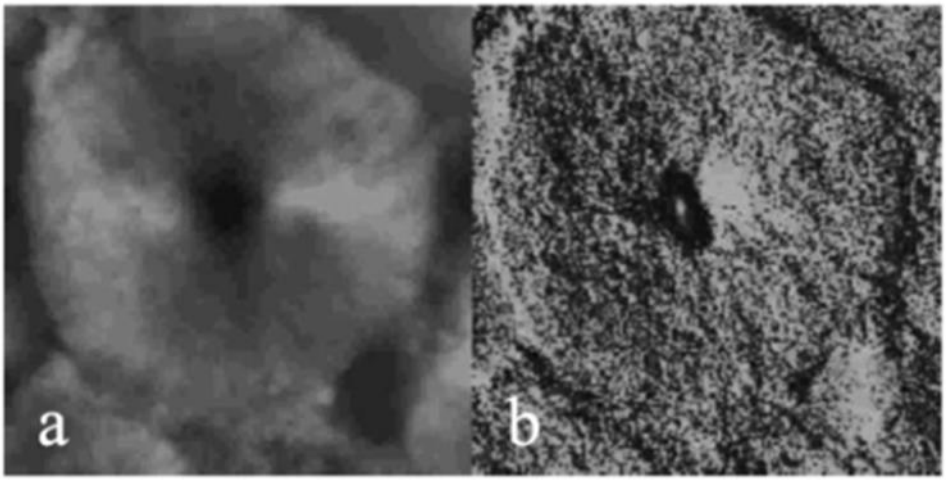

Figure 7. AFM image of a spherulite from high amylose maize starch. Image size, 10 × 10 μm; a, height image; b, phase angel shift image (Nordmark & Ziegler, 2002)

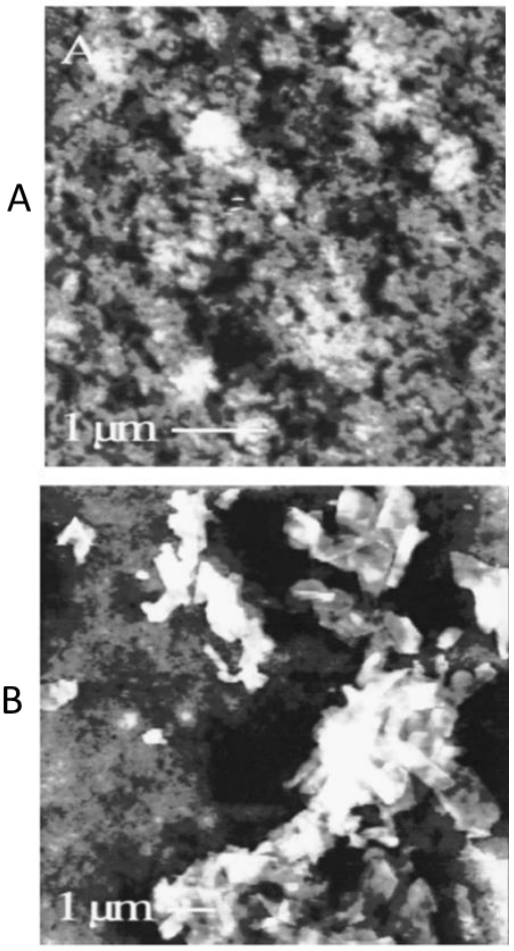

Figure 8. AFM images of the ageing process of barley starch film. (A) 1 week old (B) 5 weeks old (Kuutti et al., 1998)

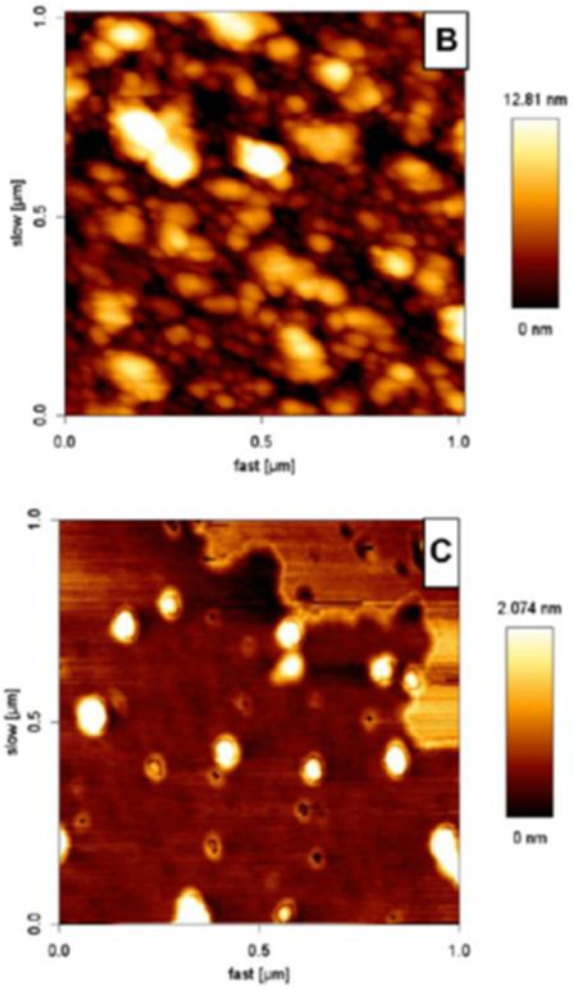

Figure 9. AFM images of potato amylose-menthone inclusion complexes using intermittent contact mode. (B) original sample; (C) diluted sample (Ades et al., 2012)

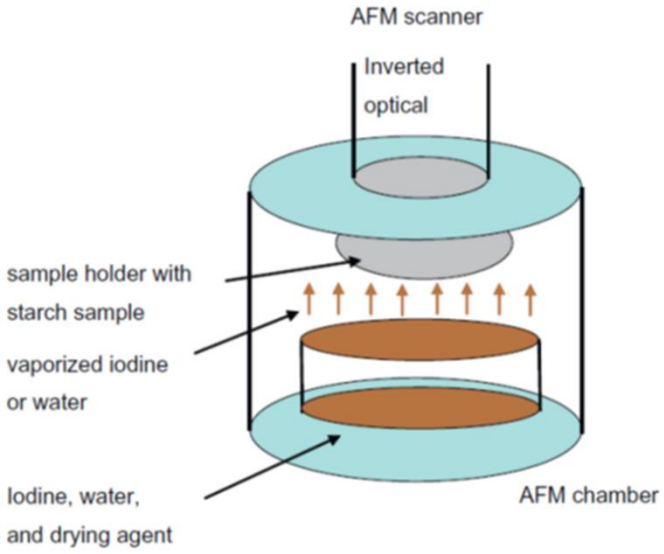

Figure 10. Schematic illustration of an environmentally controlled chamber for *in situ* AFM imaging (Park et al., 2011)

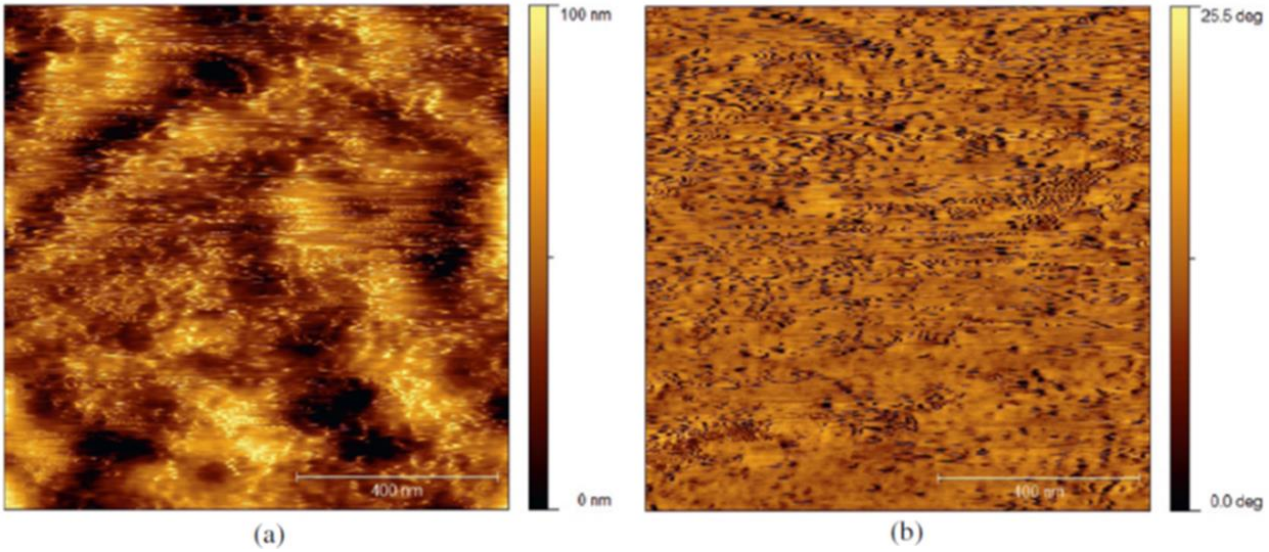

Figure 11. AFM images of potato starch exposed to iodine vapour. a, topology image; b, phase image (Park et al., 2011)

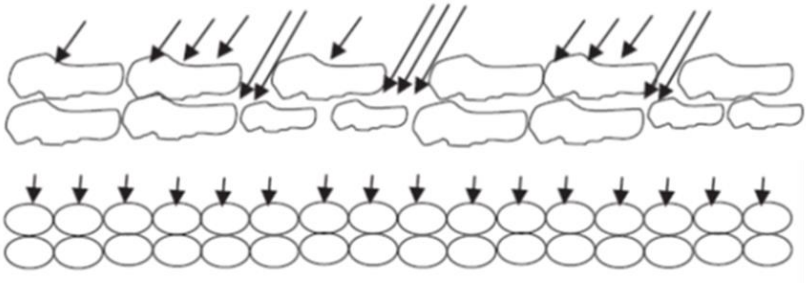

Figure 12. Schematic illustration of the formation of iodine-amylose inclusion in maize (top) and potato (bottom) starches. Blocklets of maize starch are more irregular with two size distribution. Those of potato are more uniform and circular (Park et al., 2011)

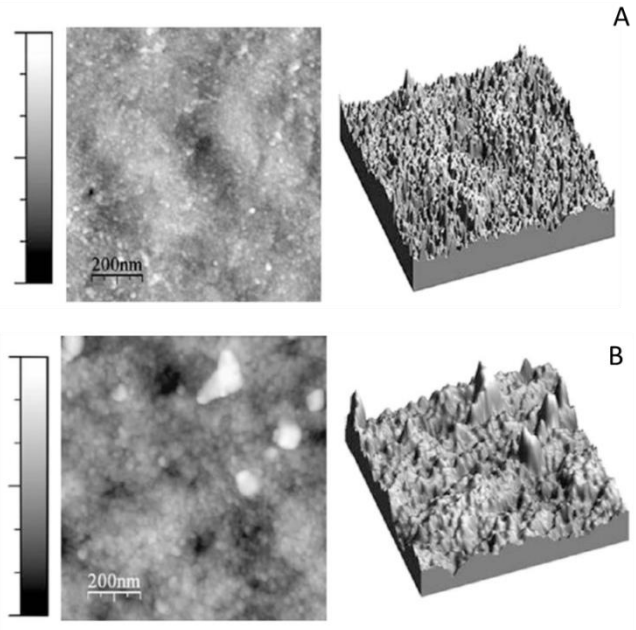

Figure 13. AFM images of surface of potato starch granules before (A) and after (B) α-amylolysis (Sujka et al., 2009)

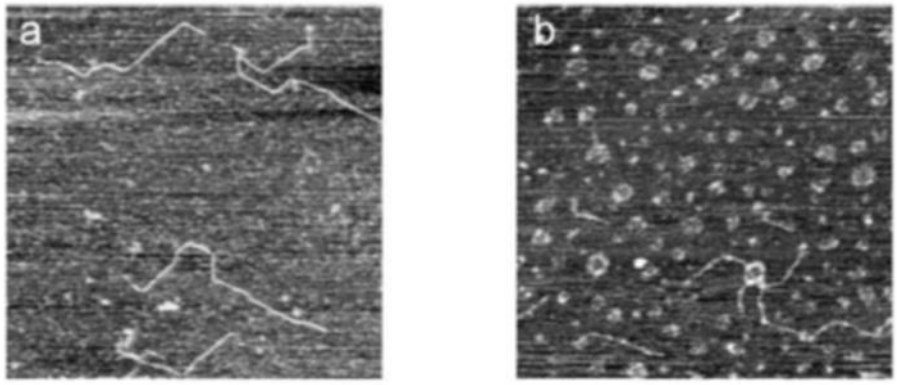

Figure 14. AFM images of pea amylose –iodine-Tween 20 complex (a) and amylose-native starch binding domain complexes (enzyme) (b) (Morris et al., 2005)

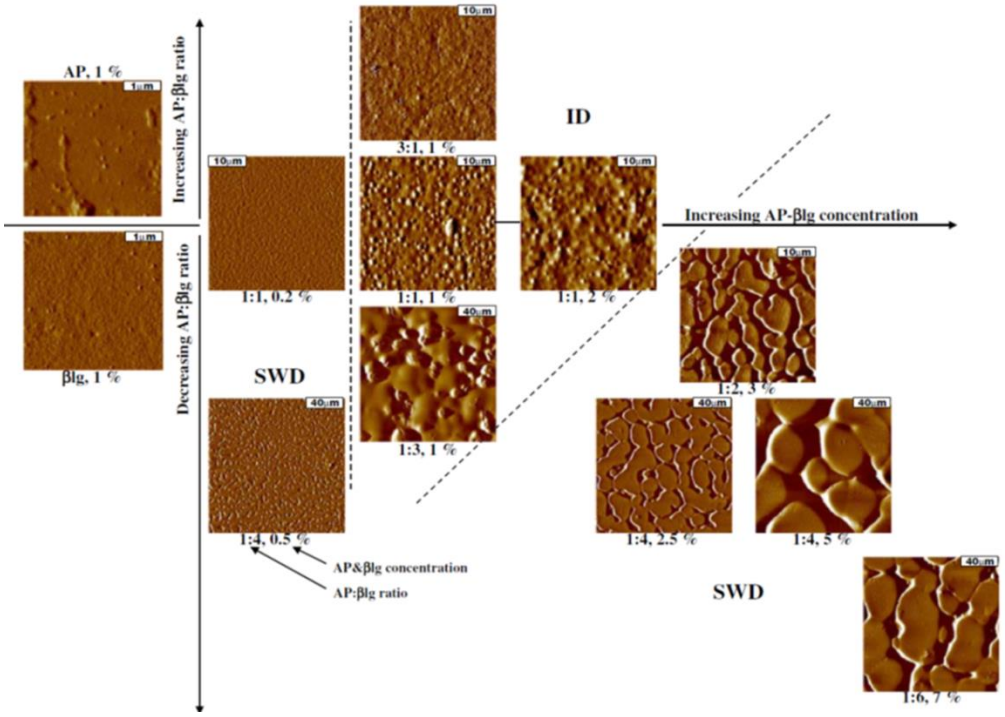

Figure 15. AFM images of film surface structure of amylopectin (AP) and β-lactoglobulin (βlg) mixtures as affected by the composition and concentration of the solution before drying (Quiroga & Bergenståhl, 2007)

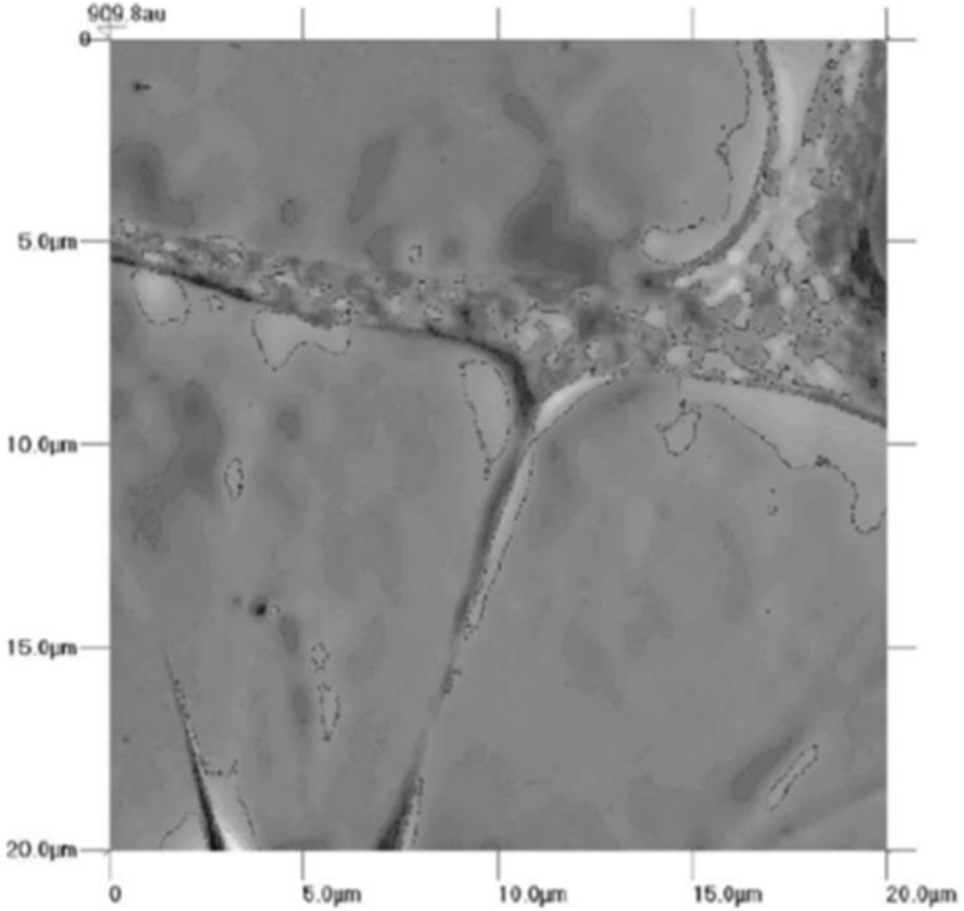

Figure 16. AFM image of starch (3%) and guar gum (1%) gel (Ptaszek et al., 2009)

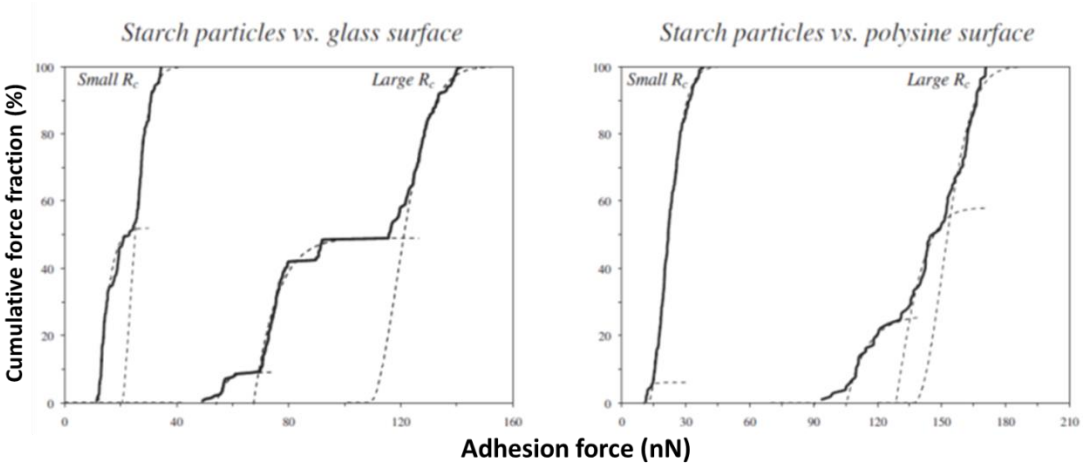

Figure 17. Distribution of the adhesion forces (nN) of surface interactions between the AFM probes with the selected wheat components particles of two large and small sizes (R_c), and the glass slide or the polysine slide. Solid lines are experimental data. Dotted lines are the fitting curves using the Weibull equation (Duri et al., 2013)